https://doi.org/10.1016/j.matchar.2021.111114
This is the Pre-Published Version.

Orientation control of phase transition and ferroelectricity in Al-doped HfO_2 thin films

Hei Man Yau[1], Xinxin Chen[1], Chi Man Wong[1], Deyang Chen[1,2,*], and Jiyan Dai [1,*]

[1]Department of Applied Physics, The Hong Kong Polytechnic University, Hung Hom, Kowloon, Hong Kong, China

[2]Institute for Advanced Materials and Guangdong Provincial Key Laboratory of Optical Information Materials and Technology, South China Academy of Advanced Optoelectronics, South China Normal University, Guangzhou 510006, China

[*]Corresponding authors:

E-mails: deyangchen@m.scnu.edu.cn (D. Chen), jiyan.dai@polyu.edu.hk (J. Dai)

© 2021. This manuscript version is made available under the CC-BY-NC-ND 4.0 license http://creativecommons.org/licenses/by-nc-nd/4.0/.

Abstract

Binary ferroelectric materials such as hafnium oxide have been intensively studied, which are expected to exhibit robust ferroelectricity comparable to the perovskite-based ferroelectrics at nanoscale. Here, using the combination of X-ray diffraction (XRD) associate with Transmission Electron Microscope (TEM), we reveal the epitaxial growth of Al-doped HfO_2 possessing various phase structures on different oriented $SrTiO_3$ substrates. The well-oriented films show different ferroelectricity indicated by piezoresponse force microscopy (PFM). The film grown on the (111) $SrTiO_3$ substrate shows the largest electromechanical effect. These results, with the analyses of structural characterizations, demonstrate the orientation control of phase transitions and ferroelectricity in Al-doped HfO_2 thin films.

Keywords: Hafnium oxide; Ferroelectric; Phase transition; thin film

1. Introduction

Bulk fluorite-structure hafnium oxide (HfO_2) is known as monoclinic phase ($P2_1/c$, m-phase) at room temperature. Although it exhibits different crystal phases (space group $P4_2/nmc$, $Fm\bar{3}m$, $P2_1/c$, Pbca, Pbcm) by increasing temperature, all these structures are centrosymmetric and non-ferroelectric. Tracing from 2011, the ferroelectricity of hafnium oxide-based films was discovered at the rare intermediate monoclinic-tetragonal phase transition [1-7], and it was reported as the result of the formation of non-centrosymmetric orthorhombic phase ($Pbc2_1$, o-phase) [3,8]. Recently, Wei *et al.* discovered a ferroelectric rhombohedral phase in well-oriented $Hf_{0.5}Zr_{0.5}O_2$ thin film [9], showing the presence of ferroelectricity in other phases besides the well-known orthorhombic polar phase ($Pca2_1$) [1]. In addition, compared to perovskite ferroelectrics, it is noted that the ferroelectric properties can be retained even grown on Si-based substrate instead of oxide single-crystalline substrates [10,11]. Thus integrating hafnium oxide into complementary metal-oxide-semiconductor (CMOS) processes is much easier as it is a well-studied CMOS-compatible dielectrics [12-15]. The ferroelectric phase of HfO_2 was discovered by Park et al. in 2013, revealing that the formation of polar o-phase is transformed from the crystallization starting with the emergence of the tetragonal phase ($P4_2/nmc$, t-phase) [16]. When the thickness of the film decreases to a certain size (~3-5 nm for pure HfO_2), the grain size will favor the ferroelectric phase due to the lower free energy, which is critically different from conventional ferroelectrics [17]. These results show the potential of hafnium oxide film on nano-scale fabrication that resolves the scaling limitation issue, promising for ultrathin ferroelectricity and non-volatile memory applications.

Apart from the thickness or grain size manipulation, the achievement of ferroelectric phase of HfO_2 can also be attained by adjusting various factors, such as dopants [3,4,18,19], electrode capping layers [20-24], strain engineering [9,25-27], oxygen vacancies [28], and electric field [29-31]. In this study, we report orientation control of phase transitions and

ferroelectricity in 10% Al-doped HfO_2 (Al:HfO_2) thin films (thickness ~ 35 nm) on different oriented $SrTiO_3$ (STO) substrates with $La_{0.7}Sr_{0.3}MnO_3$ (LSMO) as bottom electrodes. The well-oriented films show different phase structures revealed by the combination of x-ray diffraction (XRD) with transmission electron microscope (TEM) measurements. Further piezoresponse force microscopy (PFM) characterization indicates that the ferroelectric Al:HfO_2 thin films with orthorhombic phase have been obtained on STO (111) substrate. Our results offer an alternative approach to control the phase structures and ferroelectric properties in HfO_2-based thin films.

2. Experimental

Al:HfO_2/LSMO bilayers were deposited on (100)-, (110)-, and (111)-oriented STO single crystal substrates using a KrF excimer laser (Lambda Physik COMPex 205, $\lambda = 248$ nm) by pulsed-laser deposition (PLD) with a composite target of $Hf_{0.9}Al_{0.1}O_2$. Here we chose 10% Al doping HfO_2 target as either lower or higher Al content would deteriorate the ferroelectric properties. The 50-nm-thick LSMO bottom electrode was deposited at 700ºC with an oxygen pressure of 15 Pa. The laser pulse repetition rate is 2 Hz and the laser energy density is 2.5 J cm^{-2}. Then, the Al:HfO_2 film was grown on the top of LSMO layer under an oxygen pressure of 2 Pa at the same temperature with a repetition of 1 Hz. After deposition, the sample was *in-situ* annealed at 700 °C with 0.1 atm (10 kPa) O_2 for 1 hour to reduce oxygen vacancies. After that, the sample was cooled down to room temperature in the same ambient at the rate of 10 °C/min. The 50-nm-thick bottom electrode LSMO film is confirmed as metallic behavior with a good performance of transport properties [32].

The 2theta scans were carried out by x-ray diffraction (XRD, Rigaku SmartLab) to reveal the crystal structures an phase competitions of Al:HfO_2 thin films on various oriented STO substrates. The crystal profiles were further analyzed by high-resolution Field Emission Electron Microscope STEM (JEOL Model JEM-2100F) to attain the lattice parameters. The

ferroelectric properties of Al:HfO_2 thin films were probed by Piezoresponse Force Microscopy (PFM, Cypher, Asylum Research MFP-3D Infinity) equipped with a conductive Pt/Ir-coated Si tip (Nano World) with diameter of 70 nm and the cantilever with a calibrated 2.8 N/m spring constant at a free air resonance of ~75 kHz.

3. Results and Discussion

The lattice parameters of STO (100), (110) and (111) are 3.905 Å, 5.522 Å and 6.763 Å, respectively. As the lattice parameter of hafnium oxide is 5.04 Å in the cubic structure, it is experiencing a compressive or tensile strain when growing on different-oriented STO substrates. X-ray diffraction (XRD) θ-2θ patterns of Al:HfO_2/LSMO films on different oriented STO are shown in Fig. 1. The strongest intensity peak of each spectrum corresponds to the STO substrate. The featured peaks with a '*' denote the main peak of the hafnia. These XRD scans indicate various phase structures of Al:HfO_2 on STO (100), (110) and (111). Further confirmation of the orientation control of phase transitions in Al:HfO_2 thin films will be discussed in the following section according to the XRD and TEM characterizations.

In Fig. 1, The film deposited on (100)-orientation shows two peaks at 28.25° and 33.48°. Although two peaks are close to the well-known m($\bar{1}11$) and m(200) peaks representing a monoclinic structure of HfO_2 [33], the second peak also matches the o(002) structure with the d_{001}=5.269Å. To further determine the lattice parameter and the crystal structure grown on STO(100), we performed transmission electron microscopy (TEM) studies. As shown in Fig. 2, it shows a low-magnification cross-sectional TEM image of the Al:HfO_2 (~ 35 nm)/LSMO (~ 50 nm) films on STO substrate. Epitaxial growth of LSMO on STO with sharp interface is confirmed (also illustrated by selected area electron diffraction in Fig. 2(b)). High-resolution TEM image of the Al:HfO_2 film on LSMO layer, as shown in Fig. 2(c), reveals a textured polycrystalline growth of Al:HfO_2. With the support of XRD spectrum, one can note that Al:HfO_2 is not randomly orientated. From Fig. 2(c), large grains can be observed with preferred

orientation. By combining the SAED and enlarged TEM image (Fig. 2(b) & (d)), a relatively large lattice constants (a = 5.226Å, b = 5.04Å, c = 5.3Å) with c-axis along the film normal direction growth are confirmed.

Next, we turn to the study of Al:HfO_2 thin film grown on STO(110). According to XRD results in Figure 1, the peaks appear at 2θ = 28.3° and 58.27°. It is interesting to notice that these two peaks not only match the monoclinic phase m($\bar{1}11$) and m($\bar{2}22$), but also another orthorhombic Pmnb phase-o(002) and o(200). Dissimilar to the conventional ferroelectric o-phase, this phase was identified as the cotunnite-type structure, and it has a relatively large parameter along c-axis, i.e., c = 6.283Å. Yet, it is a non-ferroelectric phase similar to monoclinic phase due to the centrosymmetry. The crystal structure of Al:HfO_2 grown on STO(110) is further classified as non-ferroelectric structure microscopically from the TEM results. One can see from the contrast of the image shown in Fig.3(a) that the film is under a large strain state induced by the substrate. (111)-oriented film was deposited on the (110)-oriented STO substrate, with the d-spacing of 2.99Å along the out-of-plane direction; while it shows a (110)-oriented in-plane along the $(001)_{STO}$ direction. In Fig.3(b-c), it reveals the presence, at the interface with LSMO, of the film that is a different phase in contrast to the rest of the Al:HfO_2 film. The results of t-phase are different from that of XRD. As mentioned by Wei[1], it is believed that the interfacial Al:HfO_2 t-phase is completely strained to the substrate corresponding to a huge in-plane tensile stress of lattice mismatch. When thickness increases, the m-phase starts to emerge and becomes the majority phase of Al:HfO_2 film. Hence, the difference between XRD and TEM results can be explained.

On the other hand, ferroelectric o(002) peak of Al:HfO_2 film on STO(111) is detected by XRD. As shown in the TEM images (Fig. 3(d-f)), the film has a column-like growth with a strong preferred orientation. From the HRTEM image, we deduce the d-spacing (d_{002}) is 2.53Å, which is consistent with the XRD results. The lattice parameters of Al:HfO_2 film on STO(111)

are thus determined as a = 5. 36Å, b = 4.66Å, c = 5.06Å, where in-plane lattice is slightly distorted from substrate mismatch. Notably, most of the film depositions follow the orientation of the substrate using PLD, but Al:HfO_2 film shows a different way because of the clamping effect of the substrate.

Figure 4 shows the piezoresponse force microscopy response of Al:HfO_2 films deposited on three different oriented STO substrate. For all the films, the measured off-field butterfly loops and corresponding 180° flipped hysteresis loops at the minimum amplitude show ferroelectric characteristics. The out-of-plane PFM images of the Al:HfO_2 film also point to its ferroelectric polarization switching after applying external voltage of ±10 V. For the Al:HfO_2 thin film deposited on STO (111), the 180° phase contrast and domain structure written on the film as well as the minimum amplitude in the boundary reveal the domain structure with antiparallel polarizations as shown in Figure 4(c-e).

PFM images for Al:HfO_2 films on STO (100) and STO (110) also show the similar results to that of STO(111), as shown in Fig 5. It is obvious that Al:HfO_2 on both (100)- and (111)-oriented STO show ferroelectric properties in PFM response due to the presense of ferroelectric o-phase. Interestingly, the m-phase dominated Al:HfO_2 film on STO (110) also shows ferroelectric behevior, as shown in Fig.1. These results suggest that a small portions of ferroelectric o-phase may be present in the films grown on STO (110) while the fraction is relatively small to be detected by XRD. This claim can be supported by PFM results (see Fig. 1(a)). It is remarkable to notice in Fig. 1(a) that the magnitude of the hysteretic amplitude loop of Al:HfO_2 on STO(111) is relatively higher than the others, while that of STO(110) is the lowest. This difference can be attributed to the different ferroelectric properties induced by different lattice strain conditions.

Conclusions

In summary, phase transitions have been induced by growing ~ 35 nm-thick Al-doped HfO_2 thin films on different orientated STO substrates, leading to various ferroelectric properties. XRD and TEM measurements reveal the coexistence of monoclinic and ferroelectric orthorhombic phases on STO (100) substrate, while the films on STO (110) substrate exhibit mixed monoclinic and non-ferroelectric orthorhombic phases. Ferroelectric orthorhombic phase is formed in Al-doped HfO_2 on STO (111) substrate, which shows strong and reversible ferroelectricity observed using PFM. Therefore, this work demonstrates the substrate orientation driven phase transitions and tuned ferroelectric properties in Al-doped HfO_2 thin films, providing an alternative approach to manipulate the crystal structure and ferroelectric performance of HfO_2-based ferroelectrics.

Acknowledgments

This work was supported by the Research Grants Council of Hong Kong (Project No. 15300619). D.C. thanks the financial support from the National Natural Science Foundation of China (Grant Nos. U1832104 and 91963102) and Guangdong Science and Technology Project-International Cooperation project (Grant No. 2019A050510036). This research is also funded by the Hong Kong Scholars Program (Grant No. XJ2019006).

References

[1] J. Mueller, T. S. Boescke, U. Schroeder, S. Mueller, D. Braeuhaus, U. Boettger, L. Frey, and T. Mikolajick, Ferroelectricity in Simple Binary ZrO_2 and HfO_2, Nano Lett 12 (2012) 4318- 4323.

[2] M. H. Park, T. Schenk, C. M. Fancher, E. D. Grimley, C. Zhou, C. Richter, J. M. LeBeau, J. L. Jones, T. Mikolajick, and U. Schroeder, A comprehensive study on the structural evolution of HfO_2 thin films doped with various dopants, J. Mater. Chem. C 5 (2017) 4677-4690.

[3] T. S. Boescke, J. Mueller, D. Braeuhaus, U. Schroeder, and U. Boettger, Ferroelectricity in hafnium oxide thin films, Appl. Phys. Lett. 99 (2011) 102903.

[4] S. Mueller, J. Mueller, A. Singh, S. Riedel, J. Sundqvist, U. Schroeder, and T. Mikolajick, Incipient Ferroelectricity in Al-Doped HfO_2 Thin Films, Adv. Funct. Mater. 22 (2012) 2412.

[5] S. Mueller, C. Adelmann, A. Singh, S. Van Elshocht, U. Schroeder, and T. Mikolajick, Ferroelectricity in Gd-doped HfO_2 thin films, ECS J. Solid State Sci. Technol 1 (2012) N123.

[6] J. Mueller, U. Schroeder, T. S. Boescke, I. Mueller, U. Boettger, L. Wilde, J. Sundqvist, M. Lemberger, P. Kuecher, T. Mikolajick, and L. Frey, Ferroelectricity in Yttrium-doped Hafnium Oxide, J. Appl. Phys. 110 (2011) 114113.

[7] T. D. Huan, V. Sharma, G. A. Rossetti, Jr., and R. Ramprasad, Pathways towards ferroelectricity in hafnia, Phys. Rev. B 90 (2014) 064111.

[8] X. Sang, E. D. Grimley, T. Schenk, U. Schroeder, and J. M. LeBeau, On the Structural Origins of Ferroelectricity in HfO_2 Thin Films, Appl. Phys. Lett. 106 (2015) 162905.

[9] Y. Wei, P. Nukala, M. Salverda, S. Matzen, H. J. Zhao, J. Momand, A. S. Everhardt, G. Agnus, G. R. Blake, P. Lecoeur, B. J. Kooi, J. Iniguez, B. Dkhil, and B. Noheda, A Rhombohedral Ferroelectric Phase in Epitaxially Strained $Hf_{0.5}Zr_{0.5}O_2$ thin films, Nat. Mater. 17 (2018) 1095.

[10] S. S. Cheema, D. Kwon, N. Shanker, R. dos Reis, S. L. Hsu, J. Xiao, H. G. Zhang, R.

Wagner, A. Datar, M. R. McCarter, C. R. Serrao, A. K. Yadav, G. Karbasian, C. H. Hsu, A. J. Tan, L. C. Wang, V. Thakare, X. Zhang, A. Mehta, E. Karapetrova, R. V. Chopdekar, P. Shafer, E. Arenholz, C. M. Hu, R. Proksch, R. Ramesh, J. Ciston, and S. Salahuddin, Enhanced Ferroelectricity in Ultrathin Films Grown Directly on Silicon, Nature 580 (2020) 478.

[11] J. Lyu, I. Fina, R. Bachelet, G. Saint-Girons, S. Estandia, J. Gazquez, J. Fontcuberta, and F. Sanchez, Enhanced Ferroelectricity in Epitaxial $Hf_{0.5}Zr_{0.5}O_2$ Thin Films Integrated with Si(001) using $SrTiO_3$ Templates, Appl. Phys. Lett. 114 (2019) 222901.

[12] H. S. P. Wong, H.-Y. Lee, S. Yu, Y.-S. Chen, Y. Wu, P.-S. Chen, B. Lee, F. T. Chen, and M.-J. Tsai, Metal–Oxide RRAM, Proc. IEEE 100, (2012) 1951.

[13] M. H. Park, Y. H. Lee, T. Mikolajick, U. Schroeder, and C. S. Hwang, Review and Perspective on Ferroelectric HfO_2-Based Thin Films for Memory Applications, MRS Commun. 8 (2018) 795.

[14] F. Pan, S. Gao, C. Chen, C. Song, and F. Zeng, Recent Progress in Resistive Random Access Memories: Materials, Switching Mechanisms, and Performance, Mater. Sci. Eng. R Reports 83 (2014) 1-59.

[15] J. S. Meena, S. M. Sze, U. Chand, and T.-Y. Tseng, Nanoscale Res. Lett. **9**, 1(2014).

[16] M. H. Park, H. J. Kim, Y. J. Kim, W. Lee, T. Moon, and C. S. Hwang, Evolution of Phases and Ferroelectric Properties of Thin $Hf_{0.5}Zr_{0.5}O_2$ Films According to The Thickness and Annealing Temperature, Appl. Phys. Lett. 102 (2013) 242905.

[17] R. Materlik, C. Kuenneth, and A. Kersch, Ferroelectricity in undoped hafnium oxide, Appl. Phys. Lett. 117 (2015) 134109.

[18] S. Clima, D. J. Wouters, C. Adelmann, T. Schenk, U. Schroeder, M. Jurczak, and G. Pourtois, Identification of The Ferroelectric Switching Process and Dopant-Dependent Switching Properties in Orthorhombic HfO_2: A First Principles Insight, Appl. Phys. Lett. 104 (2014) 092906.

[19] Y. Li, J. Li, R. Liang, R. Zhao, B. Xiong, H. Liu, H. Tian, Y. Yang, and T.-L. Ren, Switching dynamics of ferroelectric HfO_2-ZrO_2 with various ZrO_2 contents, Appl. Phys. Lett. 114 (2019) 142902.

[20] Y.-C. Lin, F. McGuire, and A. D. Franklin, Realizing Ferroelectric $Hf_{0.5}Zr_{0.5}O_2$ with Elemental Capping Layers, J. Vac. Sci. Technol. B 36 (2018) 011204.

[21] Y. Goh and S. Jeon, The Effect of the Bottom Electrode on Ferroelectric Tunnel Junctions Based on CMOS-Compatible HfO_2, Nanotechnology 29 (2018) 335201.

[22] J. Wang, D. Wang, Q. Li, A. Zhang, D. Gao, M. Guo, J. Feng, Z. Fan, D. Chen, M. Qin, M. Zeng, X. Gao, G. Zhou, X. Lu, and J. M. Liu, Excellent Ferroelectric Properties of $Hf_{0.5}Zr_{0.5}O_2$ Thin Films Induced by Al_2O_3 Dielectric Layer, IEEE Electr. Device L. 40 (2019) 1937.

[23] D. Wang, J. Wang, Q. Li, W. He, M. Guo, A. Zhang, Z. Fan, D. Chen, M. Qin, M. Zeng, X. Gao, G. Zhou, X. Lu, and J. Liu, Stable Ferroelectric Properties of $Hf_{0.5}Zr_{0.5}O_2$ Thin Films within A Broad Working Temperature Range, Japan. J. Appl. Phys. 58, (2019) 090910.

[24] Y. Zhang, Z. Fan, D. Wang, J. Wang, Z. Zou, Y. Li, Q. Li, R. Tao, D. Chen, M. Zeng, X. Gao, J. Dai, G. Zhou, X. Lu, and J.-M. Liu, Enhanced Ferroelectric Properties and Insulator–Metal Transition-Induced Shift of Polarization-Voltage Hysteresis Loop in VO_x-Capped $Hf_{0.5}Zr_{0.5}O_2$ Thin Films, ACS Appl. Mater. Interfaces 12 (2020) 40510-40517.

[25] S. Estandía, N. Dix, J. Gazquez, I. Fina, J. Lyu, M. F. Chisholm, J. Fontcuberta, and F. Sánchez, Engineering Ferroelectric $Hf_{0.5}Zr_{0.5}O_2$ Thin Films by Epitaxial Stress, ACS Appl. Electron. Mater. 1 (2019) 1449.

[26] S. Liu and B. M. Hanrahan, Effects of Growth Orientations and Epitaxial Strains on Phase Stability of HfO_2 Thin Films, Phy. Rev. Mater 3 (2019) 054404.

[27] R. Batra, H. Tran Doan, J. L. Jones, G. Rossetti, Jr., and R. Ramprasad, Factors Favoring Ferroelectricity in Hafnia: A First-Principles Computational Study, J. Phys. Chem. C 121 (2017)

4139.

[28] M. Pesic, F. P. G. Fengler, L. Larcher, A. Padovani, T. Schenk, E. D. Grimley, X. Sang, J. M. LeBeau, S. Slesazeck, U. Schroeder, and T. Mikolajick, Physical Mechanisms behind the Field-Cycling Behavior of HfO2-Based Ferroelectric Capacitors, Adv. Funct. Mater. 26 (2016) 4601-4612.

[29] P. D. Lomenzo, Q. Takmeel, C. Zhou, C. M. Fancher, E. Lambers, N. G. Rudawski, J. L. Jones, S. Moghaddam, and T. Nishida, TaN Interface Properties and Electric Field Cycling Effects on Ferroelectric Si-doped HfO_2 Thin Films, J. Appl. Phys. 117 (2015) 134105.

[30] D. Zhou, J. Xu, Q. Li, Y. Guan, F. Cao, X. Dong, J. Mueller, T. Schenk, and U. Schroeder, Wake-Up Effects in Si-doped Hafnium Oxide Ferroelectric Thin Films, Appl. Phys. Lett. 103 (2013) 192904.

[31] A. Chouprik, S. Zakharchenko, M. Spiridonov, S. Zarubin, A. Chernikova, R. Kirtaev, P. Buragohain, A. Gruverman, A. Zenkevich, and D. Negrov, Ferroelectricity in $Hf_{0.5}Zr_{0.5}O_2$ Thin Films: A Microscopic Study of the Polarization Switching Phenomenon and Field-Induced Phase Transformations, ACS Appl. Mater. Interfaces 10 (2018) 8818.

[32] H. M. Yau, Z. B. Yan, N. Y. Chan, K. Au, C. M. Wong, C. W. Leung, F. Y. Zhang, X. S. Gao, and J. Y. Dai, Low-field Switching Four-state Nonvolatile Memory Based on Multiferroic Tunnel Junctions, Sci. Rep. 5 (2015) 12826.

[33] R. Ruh and P. W. R. Corfield, J. Am. Ceram. Soc. 53 (1970) 126.

FIGURE CAPTIONS

Fig. 1. XRD structural characterization of Al:HfO_2 films on LSMO-buffered (100)-, (110)- and (111)-oriented STO.

Fig. 2. Structure of Al:HfO_2/LSMO on (100)-oriented STO. (a) Low magnification TEM cross-section image of 35 nm-Al:HfO_2 on STO substrate; (b) the corresponding SAED pattern; (c) high-resolution TEM image of the Al:HfO_2/LSMO observed along [100] direction revealing a clear interface, and (d) that of Al:HfO_2 with d-spacing indications. The out-of-plane direction is $[110]_{STO}$ (zone axis). Red and orange arrows denote the direction of Al:HfO_2 and STO, respectively.

Fig. 3. Electron microscopy characterization on (110)- and (111)-oriented STO. (a,d) Low magnification TEM cross-section image, (b,e) the corresponding SAED pattern, and (c,f) high-resolution TEM image of the Al:HfO_2/LSMO on (a-c) (110)- and (d-f) (111)-oriented STO, respectively. Both zone axis of images are $\{1\bar{1}0\}_{STO}$.

Fig. 4. Piezoresponse of Al:HfO_2 film on three different oriented STO. (a) PFM amplitude and (b) phase hysteresis loops on (100)-, (110)- and (111)-oriented STO; (c) PFM out-of-plane amplitude, and (d) phase images, and (e) the corresponding line scan through the poled area for Al:HfO_2(001)/ LSMO/ STO(111) after writing an area with +10V (left) and -10V (right).

Fig. 5. PFM out-of-plane amplitude, and PFM phase image of the poled area for Al:HfO_2 films on (a-b) STO(100) and (c-d) STO(110) after writing an area with +10V (left) and -10V (right).

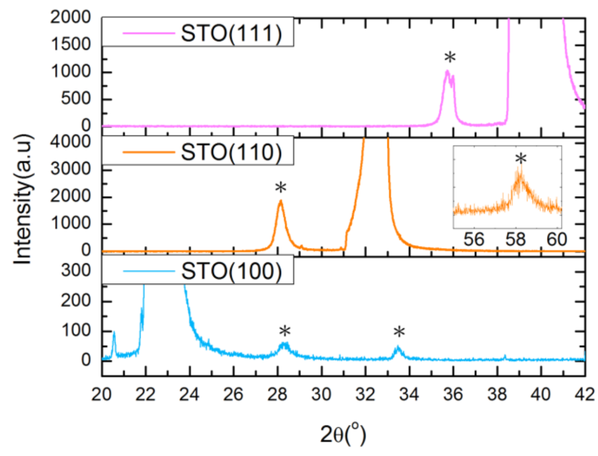

Fig.1

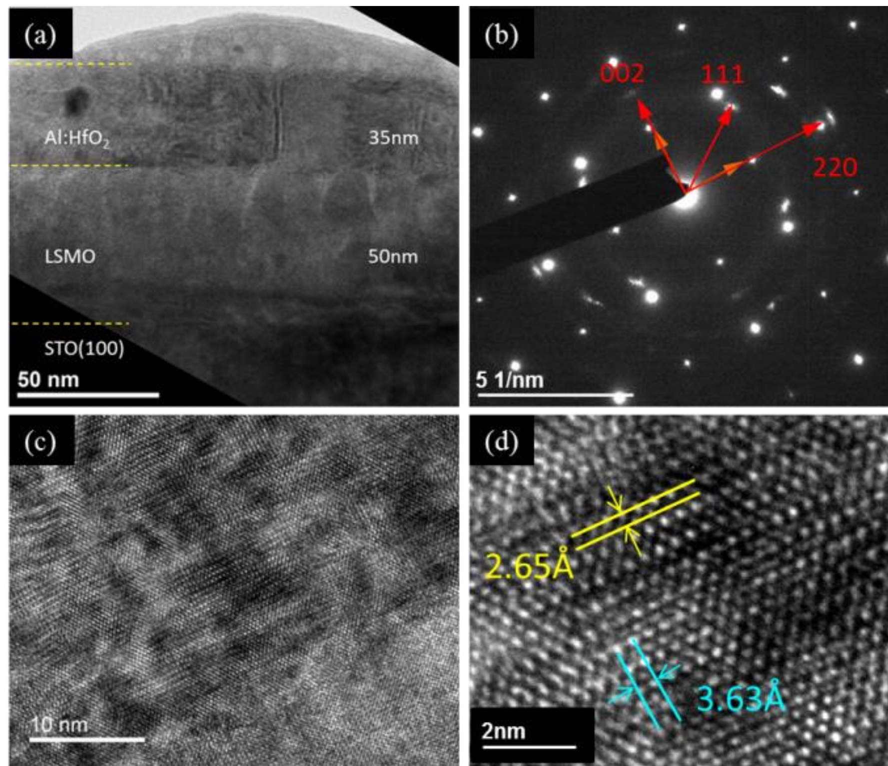

Fig.2

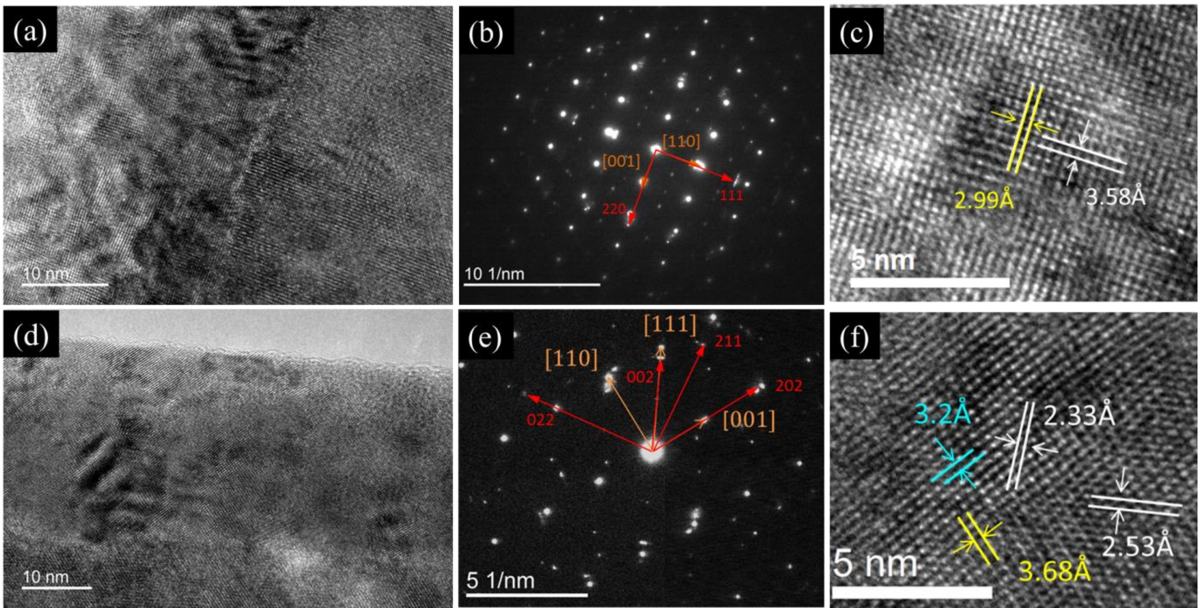

Fig.3

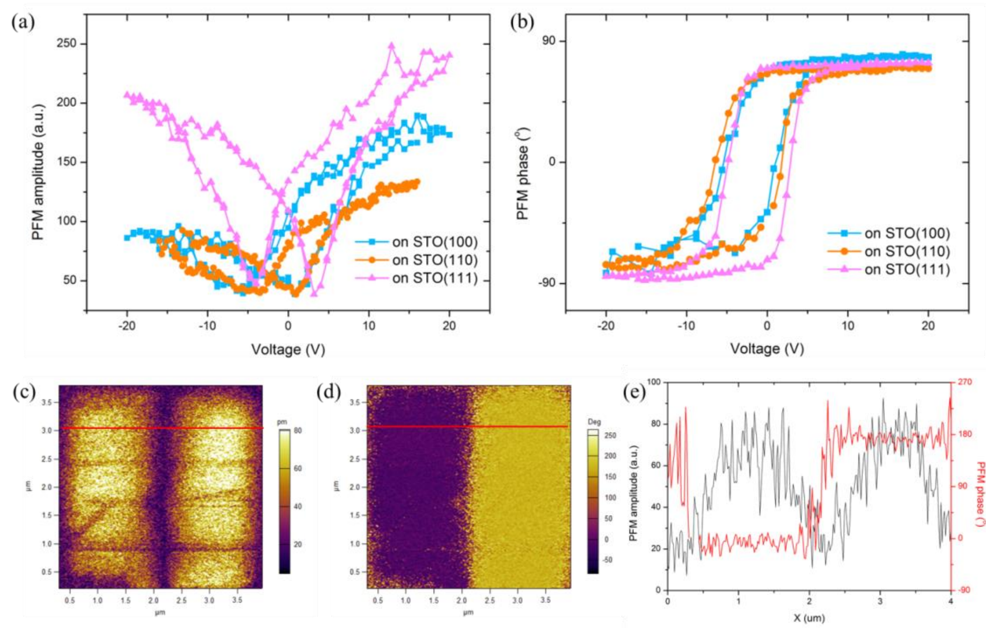

Fig.4

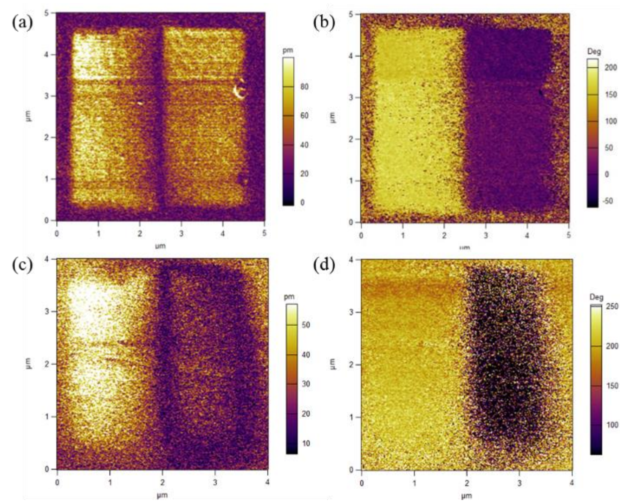

Fig.5